PHOTONICS Research

Low-cost hybrid integrated 4 × 25 GBaud PAM-4 CWDM ROSA with a PLC-based arrayed waveguide grating de-multiplexer

Lei Liu,[1,2] Limin Chang,[1,2] Yingxin Kuang,[1,2] Zezheng Li,[1,2] Yang Liu,[1,2] Huan Guan,[1] Manqing Tan,[1] Yude Yu,[1] and Zhiyong Li[1,*]

[1]*State Key Laboratory of Integrated Optoelectronics, Institute of Semiconductors, Chinese Academy of Sciences, Beijing 100083, China*
[2]*College of Materials Science and Opto-Electronic Technology, University of Chinese Academy of Sciences, Beijing 101408, China*
Corresponding author: lizhy@semi.ac.cn

We demonstrate a low-cost hybrid integrated and compact 100 GBaud four-lane coarse wavelength division multiplexing (CWDM) receiver optical sub-assembly (ROSA) based on an arrayed waveguide grating de-multiplexer in the O band. To achieve the horizontal light coupling between the planar light-wave circuit (PLC) based arrayed waveguide grating de-multiplexer and photodetector array, a 42° polished facet is applied for total reflection. A flexible printed circuit with high-frequency coplanar waveguides is used for a power supply of trans-impedance amplifier and signal transmission. The fabricated CWDM ROSA module, whose size is 18 mm × 22 mm × 6 mm, shows a 3 dB bandwidth of 21.2, 18.4, 19.6, and 19.3 GHz, respectively, in each lane. The overall symbol error rates are at a magnitude of 10^{-7} for 25 GBaud four-level pulse amplitude modulation (PAM-4) transmission with an average input optical power of 5 dBm.   © 2019 Chinese Laser Press

https://doi.org/10.1364/PRJ.7.000722

1. INTRODUCTION

With the rapid growth of data traffic in the internet data center and the fifth-generation (5G) mobile front-haul network, low-cost and high-speed receiver optical sub-assemblies (ROSAs) are of great demand and recently essential [1–7]. Compared with coherent detection, intensity-modulation direct detection is more compact, power-frugal, and cost-effective for short reach applications. Advanced modulation formats have been employed in high-speed transmission systems, such as carrier-less amplitude and phase modulation, half-cycle quadrature amplitude modulation, pulse amplitude modulation (PAM), and discrete multi-tone [8–11]. The multi-lane method is also commonly utilized in ROSA because the bandwidth requirement of opto-electronic devices can be reduced, such as in wavelength division multiplexing (WDM) and the parallel four-lane method [12–14]. For WDM technology, coarse WDM (CWDM), dense WDM (DWDM), and local area network WDM (LAN-WDM) are commonly used for multi-lane ROSA, which are compatible with the International Telecommunication Union Telecommunication Standardization Sector (ITU-T) standards [15–17]. For CWDM in the O band, the center wavelengths are 1270 nm (lane 0), 1290 nm (lane 1), 1310 nm (lane 2), and 1330 nm (lane 3), respectively. So far, 100 GbE ROSAs have been developed and applied based on silica planar

light-wave circuit (PLC) hybrid integration [18]. Arrayed waveguide grating (AWG) wavelength de-multiplexers (De-MUX) based on silica PLCs demonstrate the special advantage of low insertion loss, low-cost, large fabrication tolerance, and lower thermal sensitivity [19]. The center wavelength shift of the AWG is only 0.011 nm per centigrade, so the center wavelength drift caused by operating temperature will be less than 1.4 nm when the temperature range is −40°C to 85°C. Due to the wide wavelength spacing of the adjacent lanes of CWDM (20 nm) and the broad 3 dB bandwidth of each lane of the AWG, the requirement of wavelength accuracy and the cost of distributed feedback (DFB) laser diodes of transmitter optical sub-assembly (TOSA) will be relaxed. Thermo-electric coolers for lasers can also be removed, resulting in the total power consumption of the CWDM system being greatly reduced. Besides, polarization insensitivity of the PLC CWDM AWG will increase the responsivity of the module. Otherwise, high stability and reliability of the PLC device will increase the fabrication yield.

Vertical assemblies of a De-MUX and a photodetector (PD) have been commonly employed, but the complexity of design and assembly increased [12–14]. A 2 × 50 Gb/s (2 × 25 GBaud) ROSA has been fabricated using a transistor outline (TO) package [7]. The center wavelengths of the De-MUX are 1271 and 1311 nm. The De-MUX with a

zig-zag scheme and attached thin-film filters and mirror plane will separate and transmit the optical beams into the two-channel PDs directly. The measured four-level PAM (PAM-4) eye patterns of the ROSA are not sharp and clearly opened enough, and the measured bit error rates (BERs) are at a magnitude of 10^{-6}.

In this paper, we have demonstrated a cost-effective hybrid integrated 100 GBaud (4 × 25 GBaud) CWDM ROSA using a four-channel pin PD array and a silica-PLC-based AWG De-MUX. The silica PLC with a polished inclined surface is horizontal light coupled with the pin PD. A flexible printed circuit (FPC) board is used for high-frequency signal transmission and coupling photocurrent monitoring. The packaged ROSA is only 18 mm × 22 mm × 6 mm in size. The 3 dB bandwidths of the ROSA are 21.2, 18.4, 19.6, and 19.3 GHz, respectively, in each lane. The high qualitative eye diagrams of the ROSA indicate that the device can support high-speed transmission. The ROSA exhibits low symbol error rate (SER) when operating the SER test of four-level PAM (PAM-4).

2. ROSA CONFIGURATION

Figure 1(a) shows the structure of the CWDM ROSA. It consists of a silica-PLC AWG De-MUX integrated with a single mode fiber (SMF), a four-arrayed PD chip, a trans-impedance amplifier (TIA), an FPC board, two aluminum nitride (AlN) benches, and a metal heatsink pedestal. The four-arrayed PD chip is coupled to the PLC AWG, which is attached to the top of metalized AlN bench. The PLC of a Wooriro CWDM De-MUX AWG chip is coupled with a pigtail fiber and an SMF. The input facet of the PLC is plated with anti-reflective film to enhance the optical intensity from the SMF. The beveled facet of the PLC is polished with a 42° inclined surface. The beveled facet is then plated with Al and MgF_2 to enhance the reflectivity, especially in the case where the incident angle is smaller than the critical angle, and to protect the polished facet simultaneously. The output light beam from the bottom of the PLC will transmit to the photo-sensitive area of the PD. The TIA of an Inphi IN28xxTA is connected to the PD chip of a Broadcom D05x-HSP1x-4 and the FPC by a gold wire bonding process. Two AlN benches are adhered to the metal heat sink, which have the different thicknesses to adjust the coupling distance of the PD and PLC AWG. The thinner AlN bench is surface metalized by using chemical plating nickel and gold, which provide the common ground connecting for the TIA and FPC. The FPC contains coplanar waveguides (CPWs) for high-speed signal transmission, which can also provide a power supply for the TIA. This method achieves horizontal alignment and photoelectric conversion, resulting in low manufacturing cost and high-speed performance for ROSA.

As shown in Fig. 1(b), the terminal of the PLC is polished at an angle α, and the distance between the bottom of the PLC and the PD is d. The polished angle is 42° to reduce the Fabry–Perot resonance between the bottom of the PLC and the photo-surface of the PD. The beveled facet of the PLC is coated with reflective coating. Far field distribution of the output beam from the bottom of the PLC shows that the exit angle is 8.9°, which is simulated by using Lumerical finite-difference time-domain (FDTD) solutions. Coupling efficiency is usually used to evaluate the coupling property. We use dx and η to represent the horizontal coupling error and the coupling efficiency between PLC and PD, respectively.

As shown in Fig. 2(a), the coupling efficiency (η) is related to the distance between the PLC and PD (d). When d is 10 μm, the coupling efficiency is –0.434 dB (90.5%). When d is 50 μm, the coupling efficiency drops to be –0.899 dB (81.3%) because of the mode field extension at a longer transmission distance. We choose d to be 10 μm to consider the coupling efficiency and production yield. If d is too short, such as 1 μm or near 0 μm (PLC contact with PD), the polished end may be damaged by the productive process. Figure 2(b) shows the coupling efficiency as a function of horizontal coupling error dx when the distance between the bottom of the PLC and the PD is 10 μm for the demonstrated module configuration. At the best coupling position, the coupling efficiency will be –0.434 dB (90.5%). Compared with the best coupling position, when dx is within ±5 μm, the coupling efficiency will
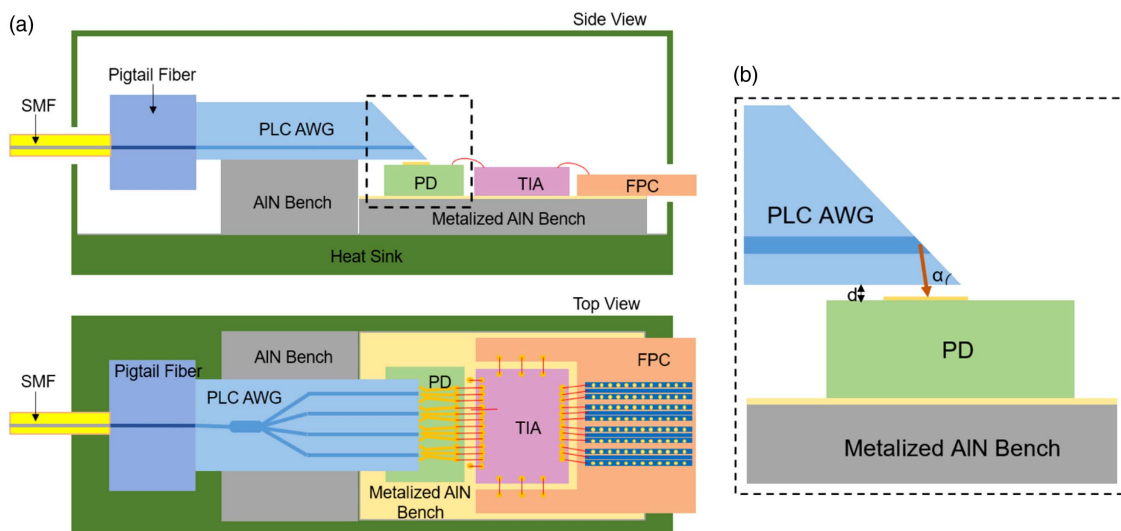

Fig. 1. (a) Side view and top view of the fabricated ROSA module; (b) side view of the coupling region.

(a)
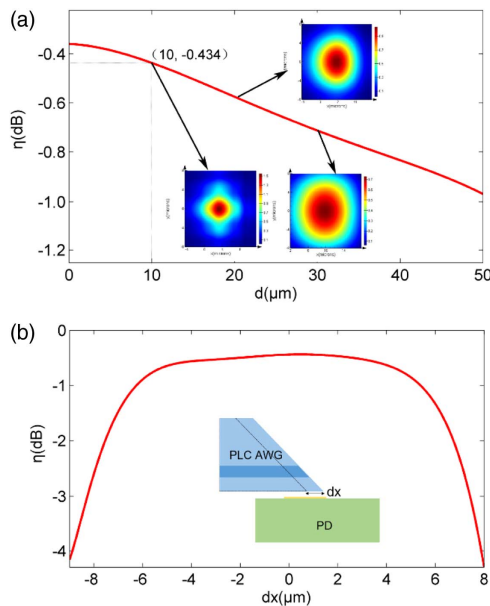

(b)

Fig. 2. Coupling efficiency (η) as a function of (a) d and (b) dx for the proposed coupling configuration.

be higher than −1 dB (79.4%), and the horizontal fabrication tolerance can be ±7 μm when the coupling efficiency is higher than −3 dB (50%).

As shown in Fig. 3, the silica-PLC AWG De-MUX chip has four CWDM lanes. The measured channel central wavelengths of the polished PLC (coupled and fixed with a pigtail and SMF) are 1271 nm (lane 0), 1290.6 nm (lane 1), 1309 nm (lane 2), and 1328.8 nm (lane 3), which are close to the wavelengths of CWDM defined by the ITU 694.2 standard. The polished AWG De-MUX has peak insertion losses of lower than 3 dB (the peak insertion losses are 2.72, 2.95, 3.23, and 2.51 dB, respectively), a high out-of-band rejection ratio of more than 35 dB, and a low crosstalk of less than −30 dB. The silica-PLC AWG De-MUX chip has a footprint size of 9.8 mm × 3 mm and a channel pitch of 750 μm. The refractive indexes of the cladding material (SiO_2) and the core material ($SiO_2 - GeO_2$) are 1.4475 and 1.4692, respectively. The PLC performance can satisfy the four-lane ROSA's requirement.
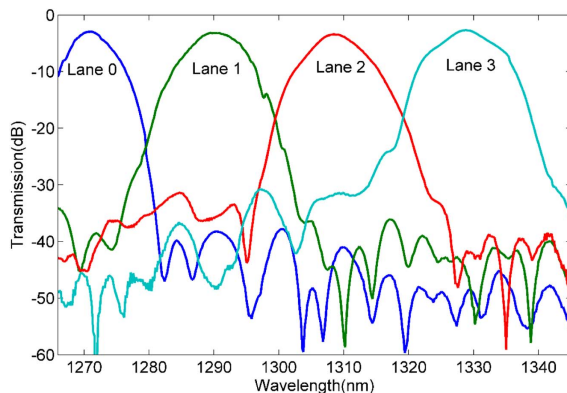

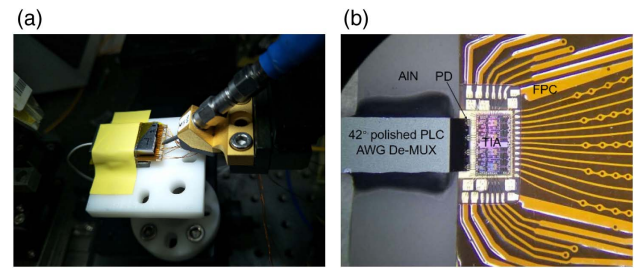**Fig. 3.** Transmission spectrum of the polished PLC AWG De-MUX coupled with an SMF.

(a)   (b)

Fig. 4. Photographs of the fabricated ROSA module with (a) the outline and (b) the internal layout.

3. ROSA FABRICATION

The ROSA fabrication processes include the assembling of the AlN benches on top of the metal heatsink, surface mounting of the PD chip, the TIA chip, and the FPC on top of AlN, wire bonding between the chips and the FPC, and light coupling of the PLC and the PD chip. The AlN benches with low thermal resistance are also used as heatsinks to conduct the heat of the PD and TIA to the bottom Cu–W heatsink. The thermal expansion coefficient and thermal conductivity of the used AlN are 4.6×10^{-6} °C^{-1} (25–300°C) and 170–200 W/mK, respectively. The TIA chip is mounted on AlN with a predetermined distance from the PD chip, which can meet the demand of wire bonding from the TIA chip to the ground plane of the surface metalized AlN. The AlN, PD, and TIA are assembled by using thermal conductive epoxy. The FPC is mounted by using conductive silver epoxy for connecting the grounds of the FPC and surface metalized AlN. After surface mounting and wire bonding, the silica PLC is coupled to the PD chip by monitoring the photocurrents of four channels transmitted by the wires of the FPC. Then, the silica PLC is fixed on the AlN bench by using ultraviolet curing adhesive. Finally, a thin metal cover is also used to protect the ROSA from dust and moisture penetration and external electromagnetic radiation. The fabricated ROSA has the size of 22 mm × 18 mm × 6 mm. Figure 4 shows the photograph of the fabricated silica-PLC ROSA module.

In order to improve the bandwidth and reduce the electromagnetic radiant crosstalk, some useful methods are applied in our work. First, grounded CPW transmission wires with a bottom ground plane are adopted in the FPC to achieve a great
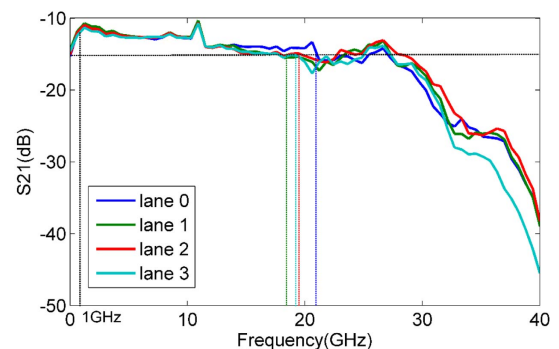

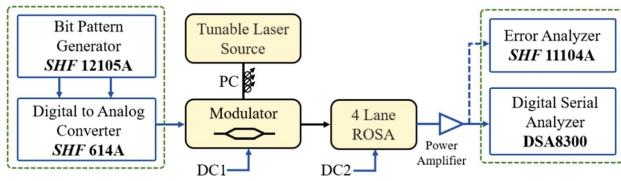**Fig. 5.** Small-signal frequency response of S21 of the ROSA module.

Fig. 6. Experimental setup of the PAM-4 eye pattern and error analysis.
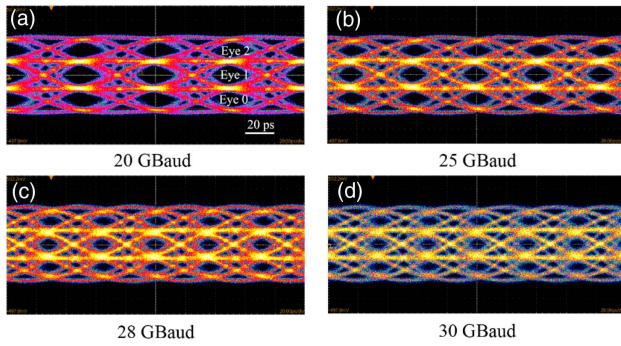

Fig. 7. PAM-4 eye patterns of the ROSA module at a Baud rate of (a) 20 GBaud, (b) 25 GBaud, (c) 28 GBaud, and (d) 30 GBaud.

ground shielded effect and high-speed signal constraint. Second, the distances of the adjacent high-speed signal wires increase gradually, to minimize the adjacent electromagnetic crosstalk. Besides, the CPW transmission lines with periodic via-holes connecting the top ground wires and the bottom ground plane are of great importance, which can introduce an appropriate inductance to adjust the characteristic impedance and reduce electric reflection and transmission loss.

4. EXPERIMENTAL RESULTS

The fabricated ROSA module was characterized by the bandwidth test, eye pattern test, and symbol error rate test at a room temperature of 25°C. The measured responsivities of the ROSA (from SMF to PD) are 0.42, 0.40, 0.37, and 0.42 A/W, respectively. The pin PD array has a 3 dB bandwidth of 22 GHz and a typical responsivity of 0.9 A/W in the O band. The total peak insertion losses of the four lanes are –3.32, –3.52, –3.86, and –3.32 dB, respectively, which include the insertion loss of the PLC AWG with fiber and the deviation of optical coupling and assembly processes. So, the degradations caused by coupling and assembly processes are 0.60, 0.58, 0.63, and 0.81 dB, respectively. The degradations of lanes 2 and 3 are worse than that of lanes 0 and 1, which may be caused by the drift of ultraviolet curing after the coupling process.

Figure 5 shows the transmission S21 parameters of four lanes of the ROSA module, where the input optical wavelengths are 1270, 1290, 1310, and 1330 nm, respectively. The small signal opto-electronic bandwidths are measured by using a 40 GHz Anritsu MS4644A vector network analyzer (VNA), a 40 Gb/s intensity modulator, and a radio frequency (RF) probe. The RF signal from the VNA is injected into the modulator. The modulated optical beam is then transmitted to the ROSA module by an SMF. The output RF signal from the FPC pads is extracted by a probe with a ground-to-signal pitch of 600 μm, as is shown in Fig. 4(a). The 3 dB bandwidths of the S21 transmission response are 21.2, 18.4, 19.6, and 19.3 GHz (reference frequency is 1 GHz, because most of TIAs include a DC block that attenuates low-frequency signals), respectively, as shown in Fig. 5. The difference of the 3 dB bandwidth may be caused by the different insertion losses of ROSA's channels and the different transmission performances of the CPWs in the FPC. The typical 3 dB bandwidths of TIA and the modulator are 25 and 30 GHz, respectively. So, the main degradation of bandwidth
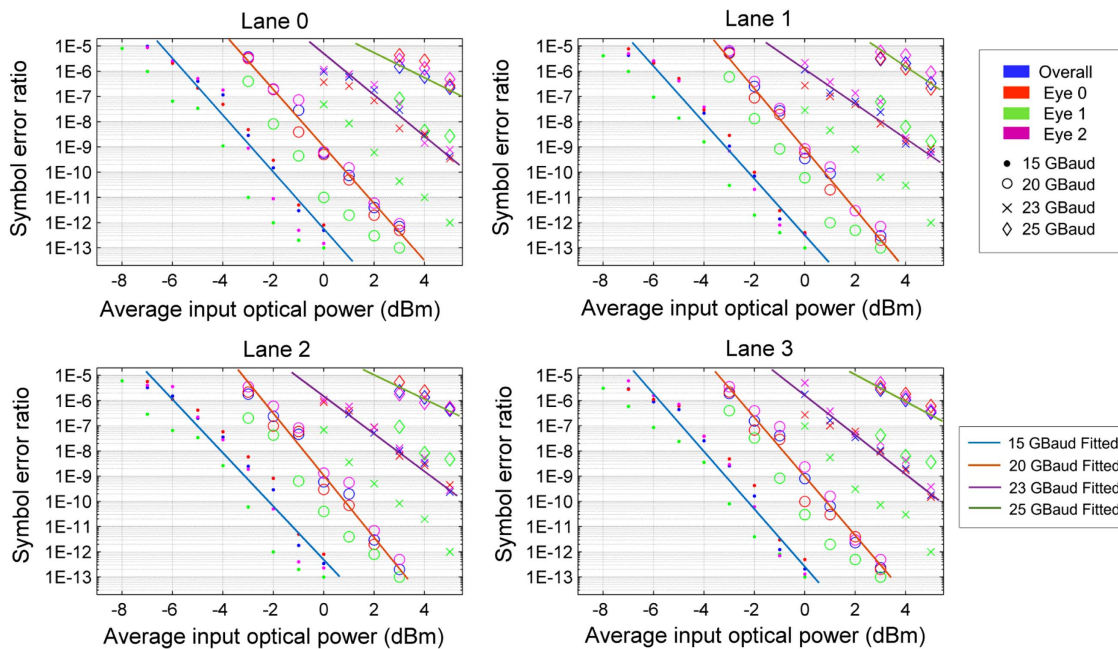

Fig. 8. Symbol error ratio of PAM-4 transmission with different Baud rates for all lanes.

may be caused by the transmission losses of the bonding golden wires (between PD, TIA, and FPC) and grounded CPWs.

The PAM-4 eye pattern is measured by using a Tektronix DSA8300 digital serial analyzer. The experimental setup of the PAM-4 eye pattern and error analysis is demonstrated in Fig. 6. An SHF 12105A bit pattern generator and an SHF 614A digital to analog converter are used to generate a PAM-4 signal. Then, eye patterns with different PAM-4 Baud rates are measured. Figure 7 shows the PAM-4 eye diagrams of different Baud rates of the ROSA module. Clearly opening eyes with minor time jitters are obtained when the average optical power is 3 dBm. Those eye patterns show fewer inter-symbol interference and noise.

Then, the PAM-4 SER is measured by using an SHF 11104A error analyzer. Figure 8 shows the symbol error ratio of PAM-4 transmission. The electric signal from each lane of the ROSA module is amplified by an SHF S807C amplifier. The amplifier with emphasis on linearity is specifically designed for multi-level signals, so that it can meet the demand of enough high signal amplitude for the SER test, especially for the closer eye levels of PAM-4. SER may be more appropriate for the PAM-4 testing using an SHF 11104A error analyzer. The error analyzer will scan the outline of the PAM-4 eyes and adjust the decision points, including the three threshold values and the uniform time delay of three PAM-4 eyes (defined in Fig. 7). Then, the error analyzer will analyze the SER of each eye one by one directly, and then obtain the overall SER. The overall SER refers to the average SER of the erring eyes, without the error-free eyes.

When the module is operated at a Baud rate of 15 GBaud, the PAM-4 overall SERs are at a magnitude of 10^{-13} with an input optical power of 0 dBm. For eyes 2, 1, and 0 (as shown in Fig. 7), the SERs for lane 0 are 1.6×10^{-13}, 0×10^{-13} (error-free, marked at 1×10^{-13}), and 8.3×10^{-13}, respectively. According to the fitted lines, the input optical powers at an overall SER of 10^{-12} will be −0.2, −0.5, −0.35, and −0.6 dBm. For 25 GBaud transmission, the PAM-4 overall SERs are at a magnitude of 10^{-7} when the average input optical power is 5 dBm, as shown in Fig. 8. With the increasing of Baud rates, the SERs are also deteriorating. Compared with other eyes of the PAM-4 eye pattern, eye 1 has the lowest SER, which is caused by the best sharpness and separation of this eye.

5. CONCLUSION

In summary, we have demonstrated a low-cost hybrid integrated and compact 100 GBaud four-lane CWDM ROSA based on an AWG De-MUX in the O band. The silica PLC AWG De-MUX and PD array are horizontally coupled by the polished facet. An FPC is used to connect the TIA and external circuit, which is optimized for high-speed transmission performance. The fabricated ROSA module has clearly opening eyes with minor time jitters at a Baud rate of 25 GBaud for each lane. The overall SERs are at a magnitude of 10^{-7} for 25 GBaud PAM-4 transmission with an average input optical power of 5 dBm. This hybrid integration is a low fabrication cost, compact, and low insertion loss method to manufacture the four-lane CWDM ROSA for a 200 or 400 GbE optical transceiver in a high-speed optical network.

APPENDIX A: GLOSSARY

WDM	wavelength division multiplexing
ROSA	receiver optical sub-assembly
PLC	planar light-wave circuit
AWG	arrayed waveguide grating
PD	photodetector
DFB	distributed feedback
TOSA	transmitter optical subassembly
FPC	flexible printed circuit
PAM-4	four-level pulse amplitude modulation
De-MUX	de-multiplexer
TIA	trans-impedance amplifier
AlN	aluminum nitride
SMF	single mode fiber
CPW	coplanar waveguide
RF	radio frequency
VNA	vector network analyzer

REFERENCES

1. J. H. Ke, Y. Gao, and J. C. Cartledge, "400 Gbit/s single-carrier and 1 Tbit/s three-carrier superchannel signals using dual polarization 16-QAM with look-up table correction and optical pulse shaping," Opt. Express **22**, 71–83 (2014).
2. Y. Zhu, K. Zou, X. Ruan, and F. Zhang, "Single carrier 400G transmission with single-ended heterodyne detection," IEEE Photon. Technol. Lett. **29**, 1788–1791 (2017).
3. M. Li, L. Zhang, L.-M. Tong, and D.-X. Dai, "Hybrid silicon nonlinear photonics [Invited]," Photon. Res. **6**, B13–B22 (2018).
4. M. Nada, M. Nakamura, and H. Matsuzaki, "25-Gbit/s burst-mode optical receiver using high-speed avalanche photodiode for 100-Gbit/s optical packet switching," Opt. Express **22**, 443–449 (2014).
5. S. Kanazawa, T. Fujisawa, N. Nunoya, A. Ohki, K. Takahata, H. Sanjoh, R. Iga, and H. Ishii, "Ultra-compact 100 GbE transmitter optical sub-assembly for 40-km SMF transmission," J. Lightwave Technol. **31**, 602–608 (2013).
6. Y. Doi, T. Ohyama, T. Yoshimatsu, S. Soma, and M. Oguma, "400-Gbps demonstration utilizing 100 GbE optical sub-assemblies and cyclic arrayed waveguide gratings," in Optical Fiber Communications Conference and Exhibition (2014), paper M2E.2.
7. S. K. Kang, J. Y. Huh, J. H. Lee, and J. K. Lee, "Low-cost and miniaturized 100-Gb/s (2 × 50 Gb/s) PAM-4 TO-packaged ROSA for data center networks," Opt. Express **26**, 6172–6181 (2018).
8. Y. Wang, J. Yu, N. Chi, and G.-K. Chang, "Experimental demonstration of 120-Gb/s Nyquist PAM8-SCFDE for short-reach optical communication," IEEE Photon. J. **7**, 7201805 (2015).
9. C. Yang, R. Hu, M. Luo, Q. Yang, C. Li, H. Li, and S. Yu, "IM/DD-based 112-Gb/s/lambda PAM-4 transmission using 18-Gbps DML," IEEE Photon. J. **8**, 7903907 (2016).
10. K. Zhong, X. Zhou, T. Gui, L. Tao, Y. Gao, W. Chen, J. Man, L. Zeng, A. P. Lau, and C. Lu, "Experimental study of PAM-4, CAP-16, and

DMT for 100 Gb/s short reach optical transmission systems," Opt. Express **23**, 1176–1189 (2015).

11. K. Zhong, X. Zhou, Y. Gao, W. Chen, J. Man, L. Zeng, A. P. T. Lau, and C. Lu, "140-Gb/s 20-km transmission of PAM-4 signal at 1.3 μm for short reach communications," IEEE Photon. Technol. Lett. **27**, 1757–1760 (2015).

12. J. Y. Huh, S. K. Kang, J. H. Lee, J. K. Lee, and S. Kim, "Highly alignment tolerant and high-sensitivity 100 Gb/s (4 × 25 Gb/s) APD-ROSA with a thin-film filter-based de-multiplexer," Opt. Express **24**, 27104–27114 (2016).

13. J. K. Lee, J. Y. Huh, S. K. Kang, and Y. S. Jang, "Analysis of dimensional tolerance for an optical demultiplexer of a highly alignment tolerant 4 × 25 Gb/s ROSA module," Opt. Express **22**, 4307–4315 (2014).

14. J. K. Lee and Y.-S. Jang, "Compact 4 × 25 Gb/s optical receiver and transceiver for 100G ethernet interface," in *International Conference on ICT Convergence* (2015), pp. 758–760.

15. T. Yoshimatsu, M. Nada, M. Oguma, H. Yokoyama, T. Ohno, Y. Doi, I. Ogawa, H. Takahashi, and E. Yoshida, "Compact and high-sensitivity 100-Gb/s (4 × 25 Gb/s) APD-ROSA with a LAN-WDM PLC demultiplexer," Opt. Express **20**, B393–B398 (2012).

16. S.-K. Kang, J. K. Lee, J. C. Lee, and K. Kim, "A compact 4 × 10-Gb/s CWDM ROSA module for 40G ethernet optical transceiver," in *60th Electronic Components and Technology Conference* (2010), pp. 2001–2005.

17. L. Soldano, J. Kubicky, D. Ton, J. Wendland, M. Allen, A. Grant, and B. Pezeshki, "Multi-wavelength 100 Gb/s silicon photonics based transceiver with silica mux/demux and MEMS-coupled InP lasers," in Optical Fiber Communications Conference and Exhibition (2017), paper Th3B.1.

18. Y. Doi, M. Oguma, M. Ito, I. Ogawa, T. Yoshimatsu, T. Ohno, E. Yoshida, and H. Takahashi, "Compact ROSA for 100-Gb/s (4 × 25 Gb/s) ethernet with a PLC-based AWG demultiplexer," in Optical Fiber Communication Conference and Exposition and the National Fiber Optic Engineers Conference (2013), paper NW1J.5.

19. T. Ohyama, Y. Doi, W. Kobayashi, S. Kanazawa, K. Takahata, A. Kanda, T. Kurosaki, T. Tanaka, T. Ohno, H. Sanjoh, and T. Hashimoto, "Compact hybrid integrated 100-Gb/s transmitter optical sub-assembly using optical butt-coupling between EADFB lasers and silica-based AWG multiplexer," J. Lightwave Technol. **34**, 1038–1046 (2016).